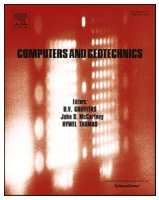
Computers and Geotechnics 147 (2022) 104773



Contents lists available at ScienceDirect

Computers and Geotechnics

journal homepage: www.elsevier.com/locate/compgeo





# The hydraulic fracturing with multiple influencing factors in carbonate fracture-cavity reservoirs

Jiangmei Qiao [a], Xuhai Tang [a,*], Mengsu Hu [b], Jonny Rutqvist [b], Zhiyuan Liu [c]

[a] State Key Laboratory of Water Resources and Hydropower Engineering Science, Wuhan University, Wuhan 430072, China
[b] Lawrence Berkeley National Laboratory, Berkeley, CA 94720, USA
[c] Research Institute of Petroleum Engineering, Sinopec Northwest Oilfield Branch, Urumqi 830011, Xinjiang, China

ARTICLE INFO

*Keywords:*
Hydraulic fracturing
Carbonate fracture-cavity reservoir
Natural cavities
Natural fractures
Confining stress

ABSTRACT

In carbonate fracture-cavity reservoirs, such as the Tahe oilfield in China, natural cavities are the main storage space of oil. It is critical to control the propagation of hydraulic fractures in order to enhance the connectivity between wellbores and oil-filled cavities. In this work, the influencing factors, including natural fracture strike angle, confining stress, the internal fluid pressure of natural cavities and fluid injection pressure are investigated numerically using the TOUGH-AiFrac simulator. Our results show that when multiple influencing factors are taken into account, natural fractures have dominant impacts on hydraulic fractures propagation, followed by the impacts of confining stress. These two influencing factors are critical to the hydraulic fracturing design in carbonate fracture-cavity reservoirs. Fluid injection pressure control can be limited by the capacity of the field equipment and the influence of cavity internal fluid pressure that tends to attract propagating fractures depending on the site-specific reservoir conditions. The present work provides guidance on how to optimize the design of hydraulic fracturing in carbonate fracture-cavity reservoirs.

## 1. Introduction

Carbonates are sedimentary rocks formed by layers of carbonate sediment laid down by marine organisms. Carbonate reservoirs produce a major portion of the world's oil and gas (Lucia et al., 1999). The Jurassic carbonate reservoirs account for large quantities of crude oil production in Saudi Arabia. The Permo-Triassic Khuff formation holds the world's largest known natural gas reserves in five Arabian Gulf countries. The Tahe oilfield located in the northern Tarim Basin in China is a typical carbonate fracture-cavity reservoir, in which the reservoir space is composed of natural cavities (dissolved caverns), dissolved pores, matrix pores and fractures (see Fig. 1). These natural fractures and cavities are the main passageway of fluid, and the natural cavities are the main storage space of oil. On the ground surface, these natural cavities might be unfilled or filled with sediment, as shown in Fig. 1(d-e). Usually, the location and geometry of natural cavities can be detected using seismic prospecting (Rapoport et al., 2004; Chalikakis et al., 2011; Xu et al., 2016) and inverse analysis technology (Wang et al., 2017; Zhang et al., 2021). Then, a procedure called targeted fracturing, is used to generate a network of fractures connecting between wellbores and natural cavities for enhanced production (Rahm, 2011; Liu et al., 2020). During this process, it is critical to understand and control the propagation of hydraulic fractures and acid fracturing (Izgec et al., 2010; Ma et al., 2018; Ali et al., 2019; Zhou et al., 2022). The present work focuses on investigating the multiple influencing factors which control the evolution of hydraulic fractures.

The prevailing confining stress has a significant influence on the propagation of hydraulic fractures, which has been studied by both experiments (Zhou et al., 2008) and numerical modeling (Tang et al., 2019). Usually, the hydraulic fractures trend to propagate and turn to the direction of the maximum principal stress. Using scaled laboratory experiments of a fractured medium, Beugelsdijk et al. (2000) observed that the hydraulic fracture geometry is influenced by the horizontal stress difference, stress regime, flow rate and discontinuity pattern. When the horizontal stress difference increases, the hydraulic fracture becomes smoother. Zhou et al. (2010) conducted fracturing experiments on rock samples with difference between the horizontal stresses, which showed that with a low difference in horizontal stresses, the hydraulic fractures propagate with many branches. Liu et al. (2014, 2018c) investigated the influence of multiple natural fractures on hydraulic fracturing experimentally and found that when the angle between the maximum horizontal stress and natural fractures is less than 45°, the

* Corresponding author.
*E-mail address:* xuhaitang@whu.edu.cn (X. Tang).

https://doi.org/10.1016/j.compgeo.2022.104773
Received 20 February 2022; Received in revised form 5 April 2022; Accepted 18 April 2022
Available online 5 May 2022
0266-352X/© 2022 Elsevier Ltd. All rights reserved.

hydraulic fractures tend to propagate along the natural fracture. Liu et al. (2018b) developed a point-based approach to improve the accuracy of stress calculation at the fracture tips of hydraulic fractures.

Understanding the influence of natural fractures is critical, since the interaction between hydraulic fractures and pre-existing fractures is a key condition for the generation of complex fracture patterns (Guo et al., 2015; Cao et al., 2020; Lu et al., 2020). In two dimensions, the interacting between hydraulic fractures and natural fractures can be divided into three categories: (1) a hydraulic fracture crosses a natural fracture; (2) a hydraulic fracture is arrested by an opening natural fracture under hydraulic pressure; (3) a hydraulic fracture is arrested by the shear slippage along a natural fracture (Blanton, 1982; Potluri et al., 2005). Unfortunately, this classification is not available for the three-dimensional (3D) problems, in which the interacting between hydraulic fractures and natural fractures is much more complex and still unsolved, because the three types of interactions might occur simultaneously. The potential of hydraulic fracture crossing a natural fracture depends on many factors, including the confining stress difference, the angle of intersection, and fluid injection scenarios (Chuprakov et al., 2014; Zhu et al., 2015). In order to predict whether a hydraulic fracture is able to be arrested by a natural fracture, Weng et al. (2011) developed a new hydraulic-fracture model to simulate complex-fracture-network propagation in a formation with pre-existing natural fractures. Their model is able to predict whether a hydraulic fracture crosses or is arrested when it encounters a natural fracture. Zhang and co-workers (Zhang et al., 2017; Zhang et al., 2019) developed a hybrid discrete-continuum numerical scheme to study the behavior of a hydraulic fracture crossing natural fractures, and showed that complex hydraulic fracture propagation patterns occur because of complicated crossing behavior during the stimulation of naturally fractured reservoirs. Hydraulic fractures mainly initiate and propagate along pre-existing natural fractures (Cipolla et al., 2010; Kresse et al., 2013). Yang and his coworkers (Zheng et al., 2019; Yang et al., 2020) developed a strength based fracturing criterion to determine the direction and length of fracture propagation in each load step effectively, which is suitable for both tensioned-sheared and compressed-sheared fractures. Luo et al. (2020) investigated the propagation of acid-etched fractures in fracture-cavity reservoirs with natural fractures and limestone caverns using the extended finite element method.

The propagation of hydraulic fractures is significantly influenced by the presence of natural cavities. Wu et al. (2004, 2011) developed a triple-continuum approach for modeling flow and transport processes in fractured rock, in which vuggy and rock matrix are main storage space of fluid. Liu et al. (2020) indicated that three main connection modes exist for natural cavities, specifically connections through straight main fractures, crooked main fractures, and pre-existing fractures.

The propagation of hydraulic fractures is also influenced by the fluid injection characteristics at injection wells. Under a low injection rate and a low fracturing fluid viscosity, the fluid tends to leak into the pre-existing discontinuities and create tortuous fracture paths following the discontinuities. De Pater and Beugelsdijk (2005) observed that, the fracture becomes smoother (less tortuous) and the interaction amount is smaller when injection rate is higher. Cipolla et al. (2010) pointed out that, when fluid injection rate is low, the tortuosity of hydraulic fractures become higher, the complexity of hydraulic fractures increases and the conductivity reduces. Ishida et al. (2012) investigated fracturing behavior of granite using water and carbon dioxide ($CO_2$) in liquid or supercritical state. They found that injecting with $CO_2$, which has a lower viscosity than water, creates a more complex fracture networks with multiple fracture branches. Zhuang et al. (2019) showed that the cracking pressure increases with the increase of the injection flow rate. Under a high injection rate and fracturing fluid viscosity, the hydraulic fractures tend to penetrate most fractures and become less tortuous (Weng et al., 2014).

The stress shadow effect, caused by the simultaneously propagation of multiple hydraulic fractures, has been extensively investigated both in laboratory experiments (Tao et al., 2021) and numerical simulations. Olson and Dahi-Taleghani (2009) used a 2D numerical model to investigate the interaction between the hydraulic fractures and natural fractures. Castonguay et al. (2013) investigated the effect of the fluid viscosity and the perforations spacing on the interaction of the multiple fractures using 3D boundary element method. Peirce and Bunger (2015) developed a numerical method to minimize the negative impact of stress shadow by adjusting the location of the perforation clusters. Salimzadeh et al. (2017) investigated the interaction of multiple hydraulic fractures propagating simultaneously using a 3D finite element model. Rayudu et al. (2019) investigated the influence of the initial angles of multiple fractures on shadow effect and the propagation of hydraulic fractures.

In this work, we investigate the influence of natural fracture strike angle, confining stress, natural cavities and fluid injection pressure on the hydraulic fracturing in carbonate fracture-cavity reservoirs. In section 2, the TOUGH-AiFrac simulator and its algorithm are briefly introduced. In section 3–6, with TOUGH-AiFrac modelling, the influence of natural fracture strike angle, confining stress, natural cavities and fluid injection pressure is discussed separately. In section 7, we discuss the propagation of hydraulic fractures under multiple influencing factors. Finally, in section 8, we provide conclusions that can help to guide and optimize the design of hydraulic fracturing in carbonate fracture-




**Fig. 1.** The Tahe oilfield, a typical carbonate fracture-cavity reservoir, is featured with a great number of natural fractures and natural cavities (provided by the Sinopec Northwest Oilfield Branch).

cavity reservoirs.

## 2. TOUGH-AiFrac simulator for hydraulic fracturing modelling

Many numerical methodologies have been developed to simulate fracturing in fractured geological media, including the finite element method (FEM), perdynamic method (Wang et al., 2016), combined finite-discrete element method (Zhao et al., 2014; Yan et al., 2016) and numerical manifold method (Yang et al., 2018; Xu et al., 2020). In this work, the TOUGH-AiFrac simulator (Tang et al., 2019) is used to model the 3D hydraulic fracturing in carbonate fracture-cavity reservoirs. This TOUGH-AiFrac simulator combines TOUGH and AiFrac, which has been successfully used to model 3D hydraulic fracturing (Tang et al., 2019), thermal cracking (Tao et al., 2020) and frost heaving cracking (Tao et al., 2021) in fractured geological media.

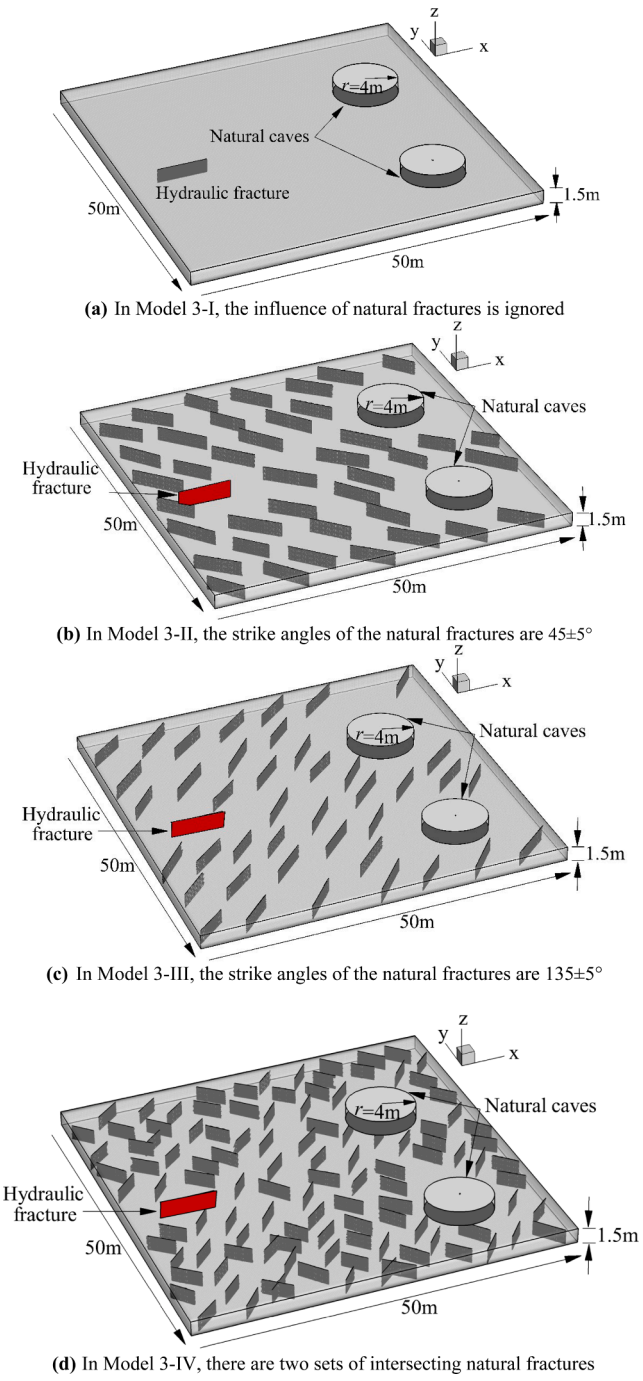
This TOUGH-AiFrac mainly consists of three components: (1) in TOUGH (Pruess et al., 2012; Rutqvist et al., 2002), the fluid flow and hydraulic pressure in porous rocks and fractures are solved; (2) in AiFrac, the mechanical deformation and stress field are solved with considering the hydraulic pressure. The two simulators are coupled in an interactive manner, an approach that has been proven successful for linking multiphase flow reservoir simulators, such as TOUGH to geomechanical simulators for the analysis of coupled processes problems in fractured rocks (Rutqvist et al., 2002; Rutqvist, 2017; Rutqvist et al., 2018). The AiFrac is developed based on the hybrid of Finite Element and Meshfree Method (FEMM) (Liu et al., 2018a), which is able to model fracturing without remeshing; (3) the hydraulic fracturing process is solved by AiFrac. The propagation direction of hydraulic fractures is solved using the point-based maximum principal stress criterion (Liu et al., 2018b) and the intersection of multiple fractures, including hydraulic fractures and natural fractures, are treated using the adaptive subelement technology.

## 3. The influence of natural fracture strike angle

In this section, the influence of natural fracture strike angle on the connection between the hydraulic fracture and natural cavities is discussed. As shown in Fig. 2, four numerical models with different natural fracture patterns are generated. The computational model domain is cuboid (50 m × 50 m × 1.5 m) with two pre-exist cavities and one hydraulic fracture. The mechanical parameters of rock matrix are set as follows: Young's modulus, $E = 30$GPa, Poisson's ratio, $\nu = 0.2$, density, $\rho = 2600$ kg/m$^3$, rock permeability, $k = 10^{-17}$m$^2$ and rock porosity, $\varphi = 0.1$. The initial length of the hydraulic fracture is 5 m, centered at (7.5, 25, 0.75). The radius of the two natural cavities is 4 m, and they are centered at (40, 37, 0.75) and (40, 13, 0.75). The cavities are assumed to be full of oil, each at an internal fluid pressure of 7.5 MPa. The fluid injection pressure is $p = 20$ MPa, which is applied on the surface of initial hydraulic fracture. In this section, the confining stress is not considered and we want to focus on investigating the impact of natural fractures strike angle on the propagation of the hydraulic fracture.

Three numerical models with different natural fracture systems are generated. In Model 3-I, there is no natural fracture. In Model 3-II and Model 3-III, there are natural fractures with different strikes and the length is set to $3 \pm 1$ m, which are chosen according to the Ref. (Lu et al., 2017; Mendez et al., 2020). Meanwhile, in Model 3-IV, there are two sets of intersecting natural fractures. In Model 3-II, the angles between the fractures and the *x*-axis are $45 \pm 5°$, and the total number of fractures is 40. In the Model 3-III, the angles between the fractures and the *x*-axis are $135 \pm 5°$, and the total number of fractures is 41. In Model 3-IV, the angles between the fractures and the *x*-axis are $45 \pm 5°$ and $135 \pm 5°$, and the total number of fractures is 111. In Model 3-II, Model 3-III and Model 3-IV, the fractures satisfy a random distribution and are perpendicular to the *xy*-plane, and the length of the fractures varies from 3 m to 5 m.

As shown in Fig. 3, in Model 3-I, without the influence of natural fractures, the hydraulic fracture propagates straightly and passes through the middle between the two cavities due to the symmetric location of the two natural cavities. Consequently, the hydraulic fracture fails to connect with any natural cavity in Model 3-I.




**(a)** In Model 3-I, the influence of natural fractures is ignored

**(b)** In Model 3-II, the strike angles of the natural fractures are 45±5°

**(c)** In Model 3-III, the strike angles of the natural fractures are 135±5°

**(d)** In Model 3-IV, there are two sets of intersecting natural fractures

**Fig. 2.** The computational models of the Model 3, in which there are two pre-existing cavities and a hydraulic fracture. The presentations of natural fractures are different in these models.

As shown in Fig. 4 (a-b) and Fig. 5 (a-b), in Model 3-II and Model 3-III, at early stage the hydraulic fracture propagates straightly under the hydraulic pressure. Then, the hydraulic fracture intersects with the pre-existing fractures, fluid flows into these fractures, and new fractures propagate from the tips of fractures. The hydraulic fractures deflect and branch because of the influence of the natural fractures.

As shown in Fig. 4 (d), when the natural fractures strike angle is 45 ± 5° relative to the *x*-axis, the hydraulic fracture connects with the

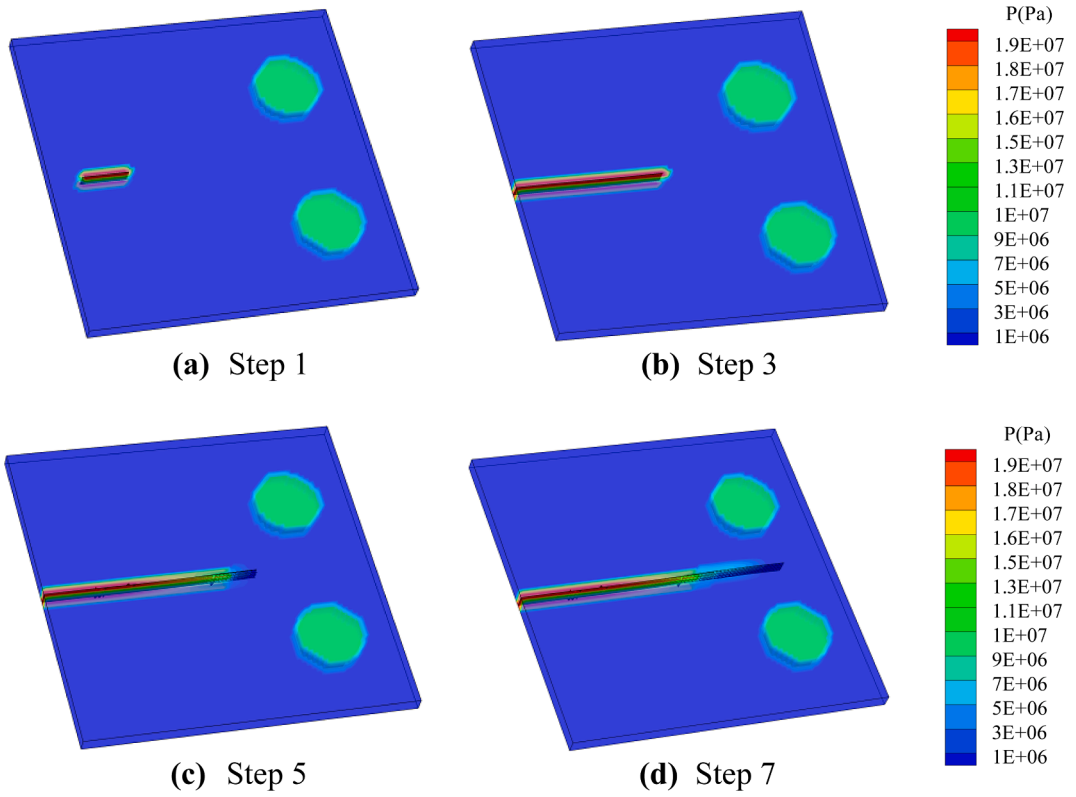



**Fig. 3.** The hydraulic fracture propagation path in Model 3-I without natural fracture.

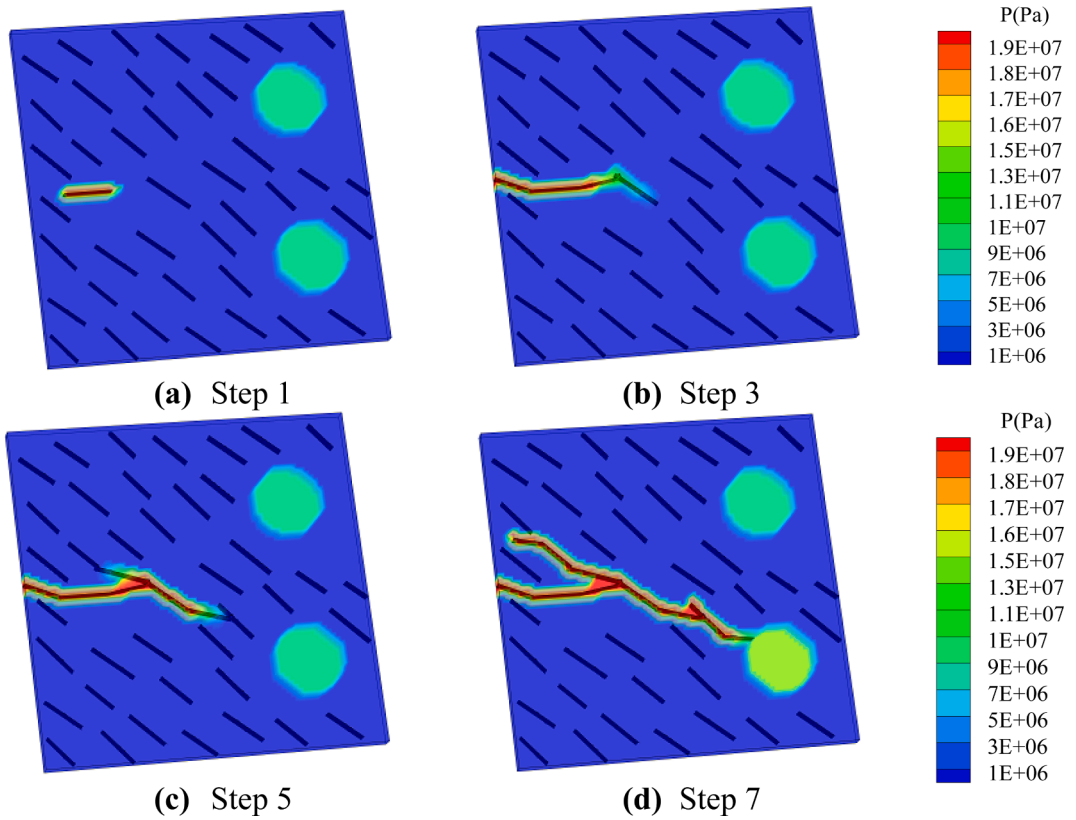



**Fig. 4.** The propagation of hydraulic fractures in Model 3-II when the natural fractures strike angle is 45 ± 5° relative to the *x*-axis.

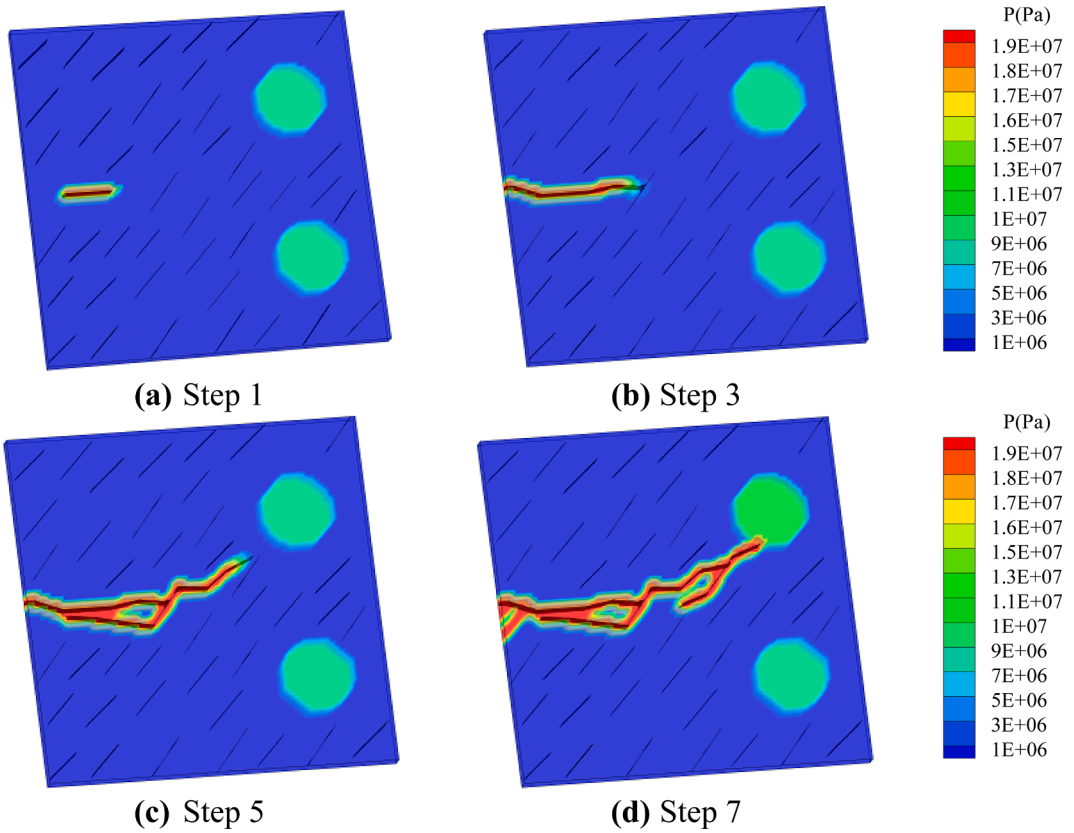



**Fig. 5.** The propagation of hydraulic fractures in Model 3-III when the natural fractures strike angle is 135 ± 5° relative to the *x*-axis.

natural cavity centered at (40, 13, 0.75). However, as shown in Fig. 5 (d), when the natural fractures strike angle is 135 ± 5°relative to the *x*-axis, the hydraulic fracture connects with the natural cavity centered at (40, 37, 0.75). Obviously, the orientation and distribution of natural fractures determine which natural cavity the hydraulic fractures are able to connect with. Thus, it is important to characterize and consider the natural fracture system in the design of hydraulic fracturing in carbonate fracture-cavity reservoirs.

As shown in Fig. 6, in Model 3-IV, the hydraulic fractures propagate and intersect with natural fractures, and finally the hydraulic fractures connect with the natural cavity centered at (40, 37, 0.75). Obviously, these hydraulic fractures deflect and branch because of the natural fractures. Because the two sets of natural fractures distribute randomly, the two pre-existing cavities have equal probability to be connected by natural fractures. Meanwhile, in field work the injection pressure at wellbore will drop down suddenly when natural cavities with low internal pressure are connected. Therefore, frequently it is only able to connect one cave.

## 4. The influence of confining stress

In this section, two numerical models are constructed to investigate the influence of confining stress on hydraulic fracture propagation, which are verified by comparing to existing experiments. In order to discuss the influence of confining stress, Model 4-I without confining stress is generated according to one experiment (Jiao et al., 2015), while Model 4-II with confining stress is generated according another experiment (Jiang et al., 2009). In either case, a hydraulic fracture is propagated from a central vertical borehole of a cubic rock sample (Fig. 7).

In Model 4-I, without confining stress, a cubic rock sample of dimension 15 cm × 15 cm × 15 cm with a central vertical borehole and a pre-existing fracture. The diameter and height of this vertical wellbore are $r = 1$ cm and $h = 9$ cm, respectively. The pre-existing fracture length, $l = 2$ cm, and oriented at an angle, $\beta = 30°$ to the *y*-axis. The Young's modulus, Poisson's ratio, density, permeability and porosity of the rock matrix are $E = 4$GPa, $\nu = 0.6$, $\rho = 1100$ kg/m$^3$, $k = 10^{-14}$ m$^2$ and $\varphi = 0.1$, respectively. During hydraulic fracturing, the water with constant fluid pressure is injected into the hydraulic fracture through the wellbore.

The Model 4-II, in which confining stress is considered, consists of a cubic rock sample with dimensions 30 cm × 30 cm × 30 cm with a central borehole and a pre-existing fracture (Jiang et al., 2009). The confining stress is set to $\sigma_H = 4$ MPa and $\sigma_h = 1$ MPa. The diameter and height of the vertical wellbore are $r = 2$ cm and $h = 25.5$ cm respectively. The pre-existing fracture has a length of $l = 3$ cm, and is oriented at an angle $\beta = 30°$ to the *y*-axis. The Young's modulus, Poisson's ratio, density, permeability and porosity of the rock are set to $E = 8.4$GPa, $\nu = 0.23$, $\rho = 1100$ kg/m$^3$, $k = 10^{-16}$m$^2$ and $\varphi = 0.018$. During hydraulic fracturing, the water with constant flow rate of $2.1 \times 10^{-9}$m$^3$/s is injected into the hydraulic fracture through the wellbore.

The numerical simulation results of Model 4-I are shown in Fig. 8. The hydraulic fracture propagates along the direction of initial hydraulic fracture and finally splits the sample into two parts. The numerical result is in good agreement with the experimental results of Jiao et al. (2015), as shown in Fig. 9.

The numerical results of Model 4-II are shown in Fig. 10. With the confining stress, the hydraulic fracture propagates from the pre-existing fracture and then turn to the direction of maximum principal stress, which finally splits the sample into two parts. The numerical results of the propagation path are compared with the experimental results of Jiang et al. (2009), as shown in Fig. 11, due to the asymmetry of the experimental results, the two curves do not exactly match.

## 5. The influence of natural cavity internal pressure

In this section, the influence of internal fluid pressure in the natural cavities on the hydraulic fracture propagation is investigated using

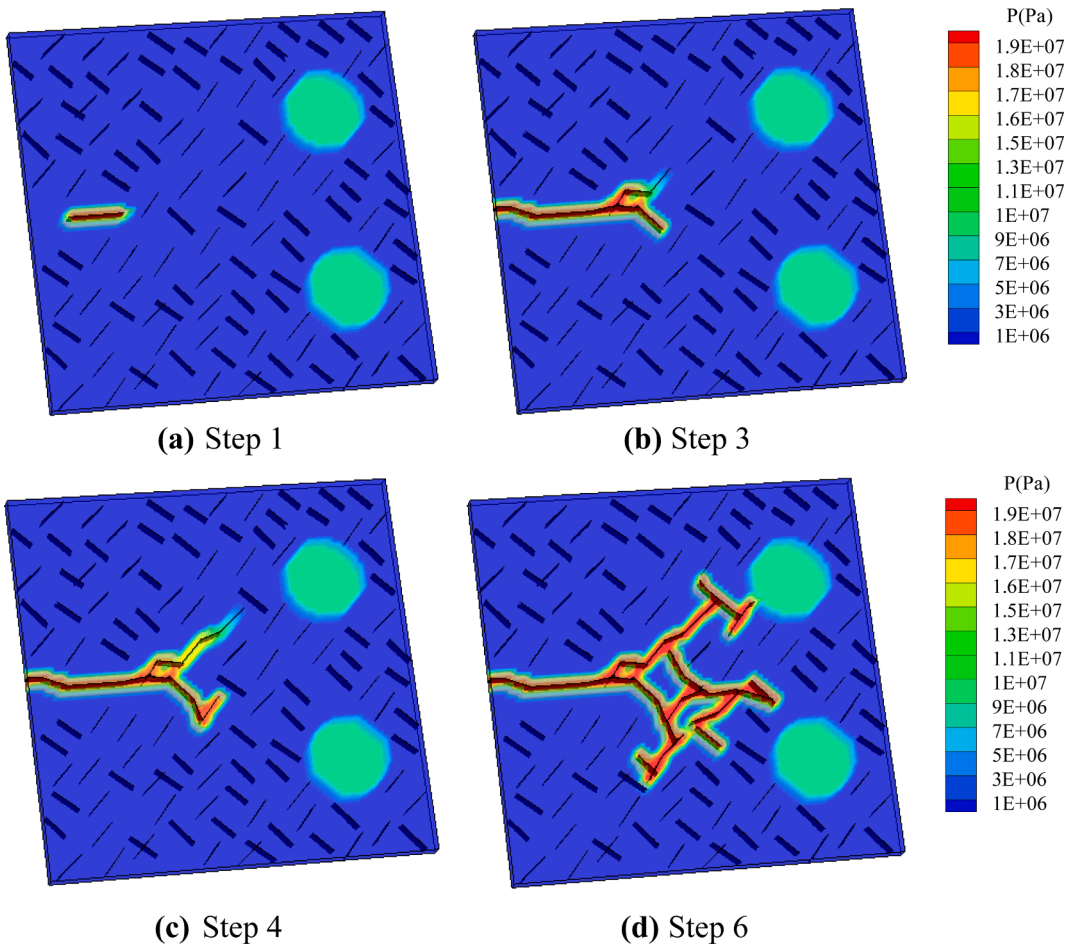



**Fig. 6.** The propagation of hydraulic fractures in Model 3-IV when there are intersecting natural fractures.

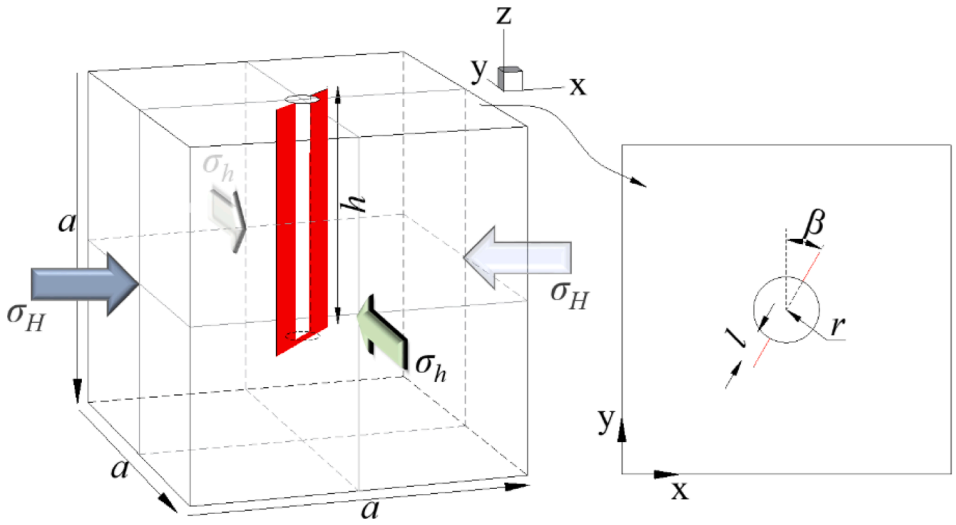



**Fig. 7.** The computational model of the Model 4-I and Model 4-II with a pre-fracture and a vertical wellbore.

TOUGH- AiFrac.

### 5.1. Single cavity

In order to investigate the influence of fluid pressure in a single natural cavity, seven numerical models are generated with different internal fluid pressures. In Model 5-I-a, the influence of natural cavity is not considered. In Model 5-I-b, six numerical models are generated with different internal fluid pressures, and the internal fluid pressures are 0 MPa, 5 MPa, 10 MPa, 15 MPa, 20 MPa, 25 MPa respectively.

In these seven numerical models, the computational model is cuboidal with dimension of 35 m × 35 m × 1.5 m. There is a single natural oil-filled cavity centered at coordinates of (25, 17, 0.75), as shown in Fig. 12. The geometry of the natural cavity is assumed circular

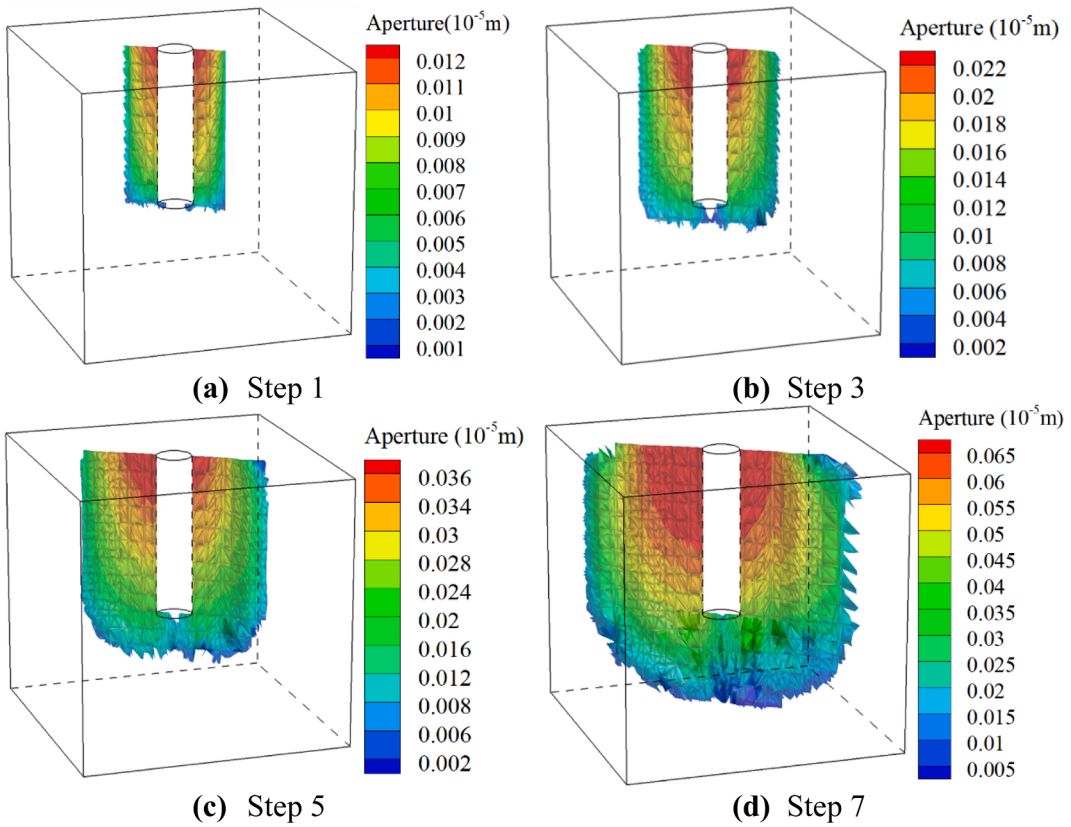



**Fig. 8.** The propagation of hydraulic fractures in Model 4-I.

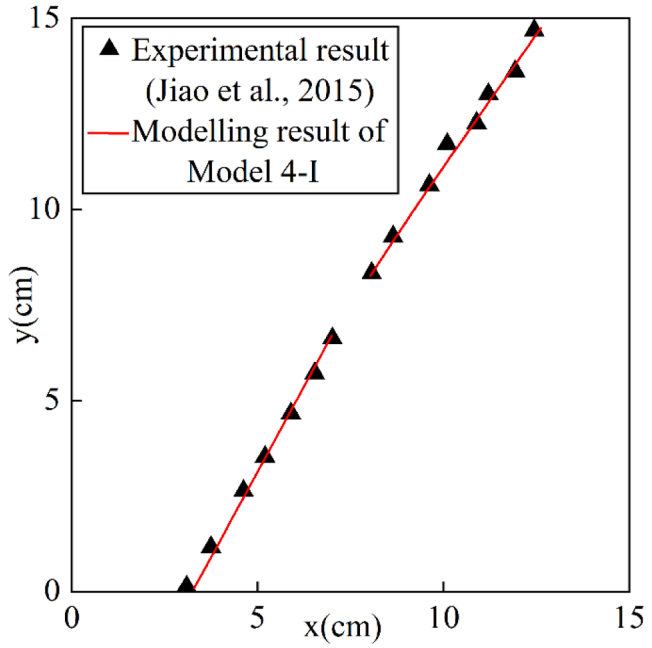



**Fig. 9.** The hydraulic propagation path of Model 4-I is consistent well with the previous experimental results (Jiao et al., 2015).

on the *xy*-plane with a radius of $r = 4$ m. An initial fracture of length 10 m along the *x*-direction is centered at (5, 23, 0.75). A constant injection fluid pressure $p = 20$ MPa is applied at the right end of this hydraulic fracture. The mechanical parameters of rock matrix are listed in Table 1, which are chosen according to the Ref. (Li et al., 2016a; Li et al., 2016b).

In Model 5-I-a, the natural cavity is not considered. The numerical results of Model 5-I-a are shown in Fig. 13. Without the influence of natural cavity, the hydraulic fracture propagates along the direction of initial hydraulic fracture.

In Model 5-I-b, the natural cavity filled with oil is taken into account. Compared to rock matrix, the Young's modules of these natural cavities is lower ($E = 5$GPa), while the permeability is higher ($k = 10^{-12}$m$^2$). The numerical results of Model 5-I-b are shown in Fig. 14. When the internal fluid pressure is small, the influence of natural cavities on the hydraulic fracture propagation is negligible and the hydraulic fracture propagates nearly straightly. When the internal pressure of the natural cavity increases, the interaction between the fracture and the cavity increases. The hydraulic fracture deflects and turns towards the natural cavities (see Fig. 15). The natural cavities with high internal fluid pressure attracts the hydraulic fracture, which leads to the increasing of deflection angles (see Fig. 14 b).

### 5.2. Double cavities

As shown in Fig. 16, in Model 5-II the computational model is cuboid with the dimension of 40 m × 30 m × 12 m. There are two oil-filled natural cavities centered at the coordinates of (14, 20, 6) and (26, 20, 6) respectively. The cavities are assumed spherical with radius $r = 4$ m. The initial length and width of hydraulic fracture are 12 m and 6 m respectively, which is located at the bottom boundary of the model. A constant fluid pressure of $p = 15$ MPa is applied on the surface of initial hydraulic fracture, while the confining stress is set to $\sigma_x = 7$ MPa, $\sigma_y = 8$ MPa and $\sigma_z = 10$ MPa. The mechanical parameters of the rock matrix are the same with that listed in Table 1.

The Model 5-II-a and Model 5-II-b are generated with different natural cavity internal pressures. In Model 5-II-a, the internal fluid pressures of two natural cavities are both set to $p = 15$ MPa. In Model 5-II-b, the internal fluid pressures of two natural cavities are set to be $p = 20$ MPa and $p = 15$ MPa respectively.

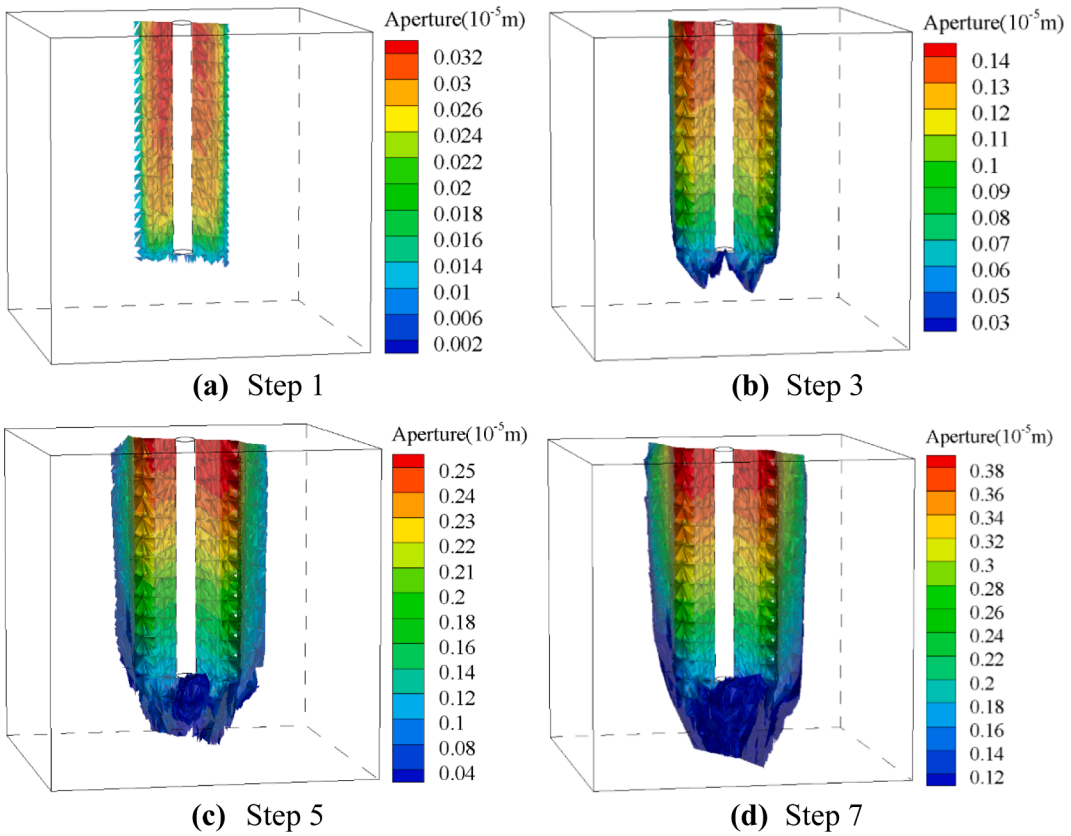



**Fig. 10.** The path of fracture propagation in Model 4-II.

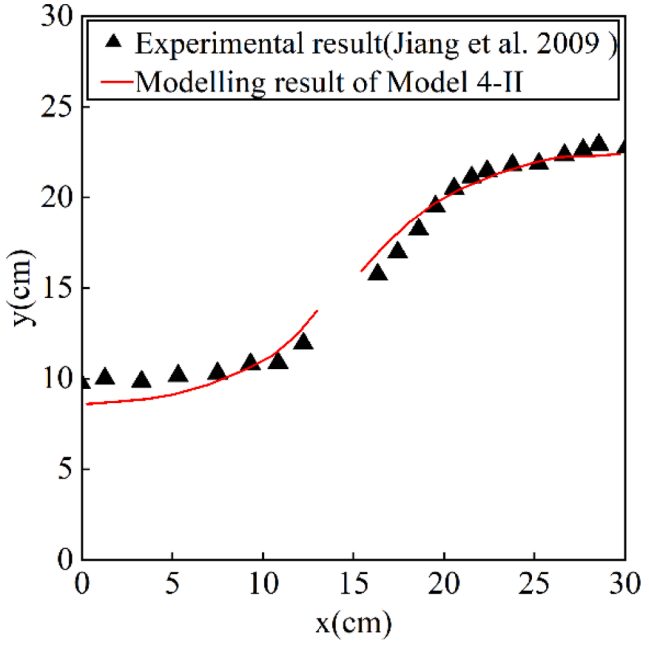



**Fig. 11.** The hydraulic propagation path of Model 4-II is consistent well with the previous experimental results (Jiang et al., 2009).

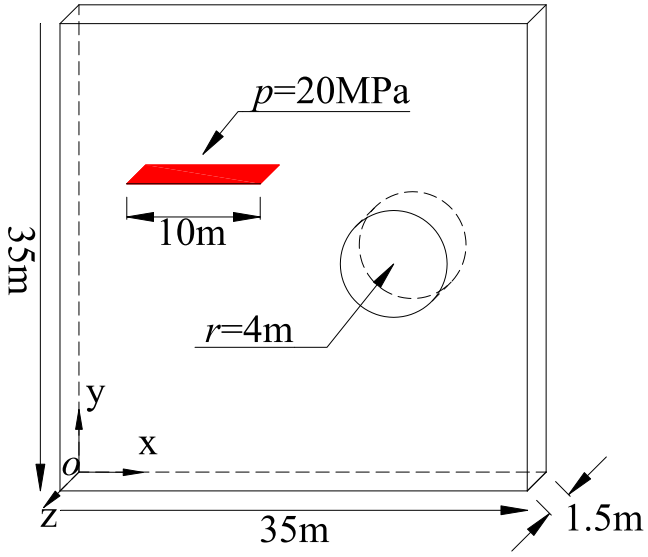



**Fig. 12.** The computational model of Model 5-I with a single natural cavity.

The numerical result of Model 5-II-a is shown in Fig. 17. Because the internal fluid pressure of the two natural cavities is same and the stress field is symmetric, the hydraulic fracture propagates straightly along the initial direction.

The numerical result of Model 5-II-b is shown in Fig. 18. Initially the hydraulic fracture propagates along the *y*-plane (see Fig. 18 a-b). Then

**Table 1**
The mechanical parameters of rock matrix.

| Input parameters | Value |
|---|---|
| Young's modulus, $E$ (GPa) | 30 |
| Poisson's ratio, $\nu$ | 0.2 |
| Density, $\rho$(kg/m$^3$) | 2600 |
| Permeability, (m$^2$) | $10^{-17}$ |
| Porosity | 0.1 |

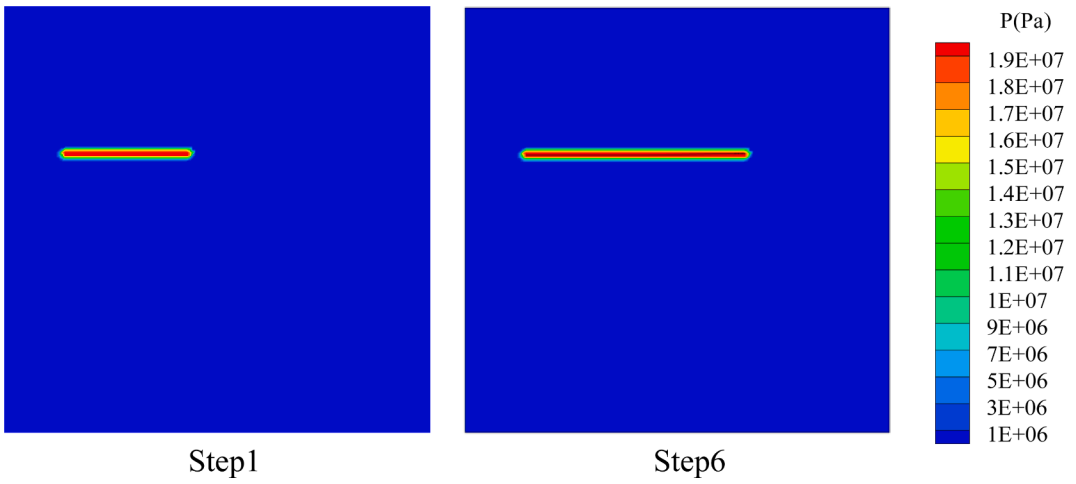
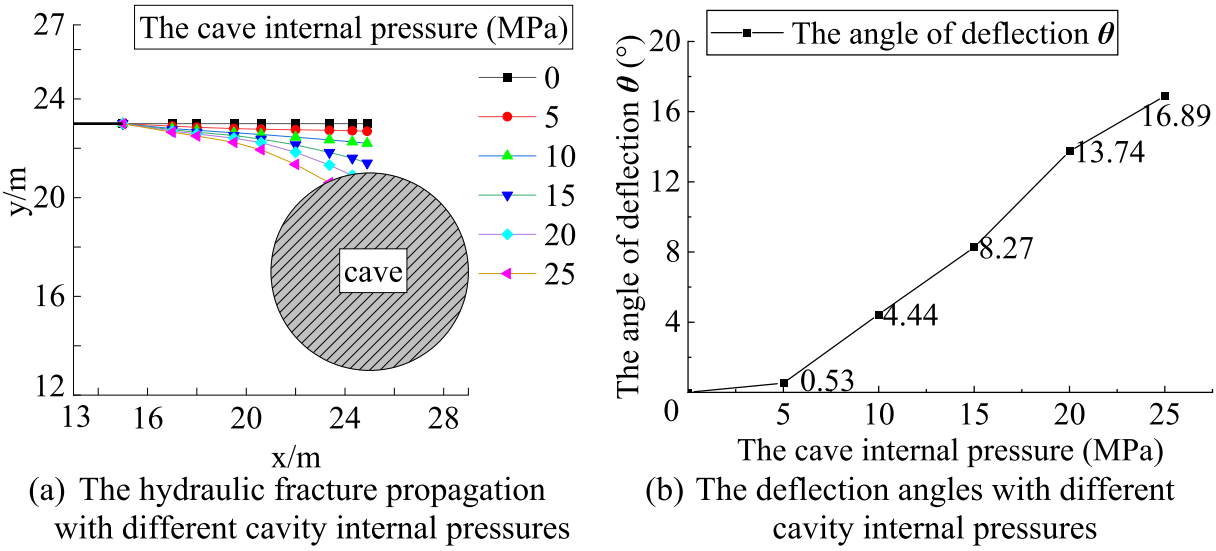



**Fig. 13.** Fracture propagation path without natural cavity in Model 5-I-a.




(a) The hydraulic fracture propagation with different cavity internal pressures

(b) The deflection angles with different cavity internal pressures

**Fig. 14.** The hydraulic fracture propagation and the deflection angles in Model 5-I-b.

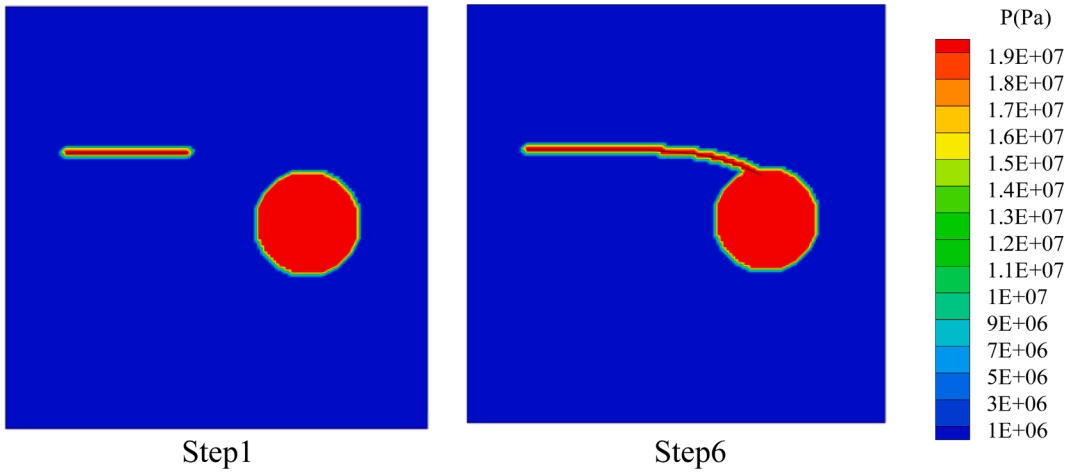



**Fig. 15.** Hydraulic fracture propagation path when the natural cavity internal pressure is 20 MPa.

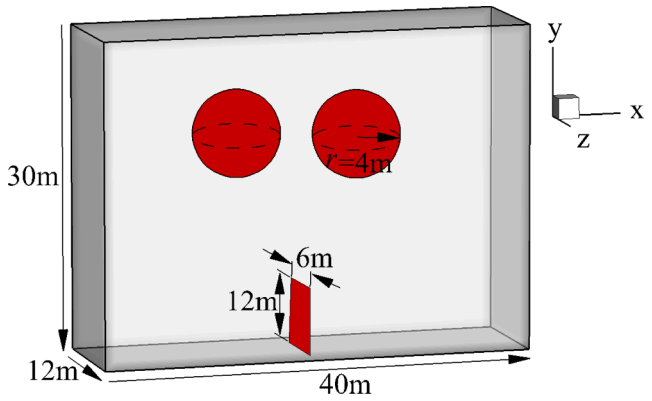



**Fig. 16.** The geometry of Model 5-II with two natural cavities.

the hydraulic fracture deflects and finally connects with the natural cavity with higher internal fluid pressure (see Fig. 18 c-d). When the internal pressure of the natural cavity increases, the interaction between the fracture and the cavity increases. The hydraulic fracture deflects and turns to the natural cavity with higher internal fluid pressure. Thus, natural cavities with high internal fluid pressure can attract propagating hydraulic fractures.

## 6. The influence of injection pressure

Injection fluid pressure at wellbores also has influence on the hydraulic fracturing, which is an operation parameter controlled by oil-field operators during the process of oil production. As shown in Fig. 19, the computational model of Model 6 is cuboid with the dimension of 8 m × 8 m × 3 m. A vertical wellbore is located at the center, and the diameter and height of this vertical wellbore are $r = 0.35$ m and $h = 2.5$ m respectively. The initial radius and depth of the initial hydraulic fracture are $R = 0.85$ m and $H = 1.5$ m respectively. There are two oil-filled cavities with the diameter of $d = 0.6$ m, and their coordinates are (3.5, 1, 1.5) and (3.5, 6, 1.5) respectively. The internal fluid pressures of these two cavities are 20 MPa. The Young's modulus, Poisson's ratio, density, permeability and porosity of the rock matrix are $E = 30$GPa, $\nu = 0.2$, $\rho = 2600$ kg/m$^3$, $k = 10^{-17}$m$^2$ and $\varphi = 0.1$ respectively. The confining stress is set to be $\sigma_x = 7$ MPa, $\sigma_y = 8$ MPa and $\sigma_z = 10$ MPa.

Two computational models, Model 6-a and Model 6-b, with different injection fluid pressures are generated. The constant injection fluid pressure of $p = 15$ MPa is applied on the initial hydraulic fracture surface in Model 6-a. The constant injection fluid pressure of $p = 20$ MPa is applied on the initial hydraulic fracture surface in Model 6-b.

The numerical results of Model 6-a are shown in Fig. 20. With the low injection fluid pressure, the hydraulic fracture propagates and turns to the direction of maximum principal stress in $z$-direction. Finally, the hydraulic fracture fails to connect with any cavity in Model 6-a. The numerical results of Model 6-b are shown in Fig. 21. With the high injection fluid pressure, the hydraulic fracture propagates approximately straightly and the influence of confining stress decreases. Finally, the hydraulic fracture successes to connect with the two cavities in Model 6-b. Compared Model 6-a and Model 6-b, the higher injection fluid pressure is able to reduce the tortuosity of hydraulic fracture, and reduce the influence of confining stress meanwhile.

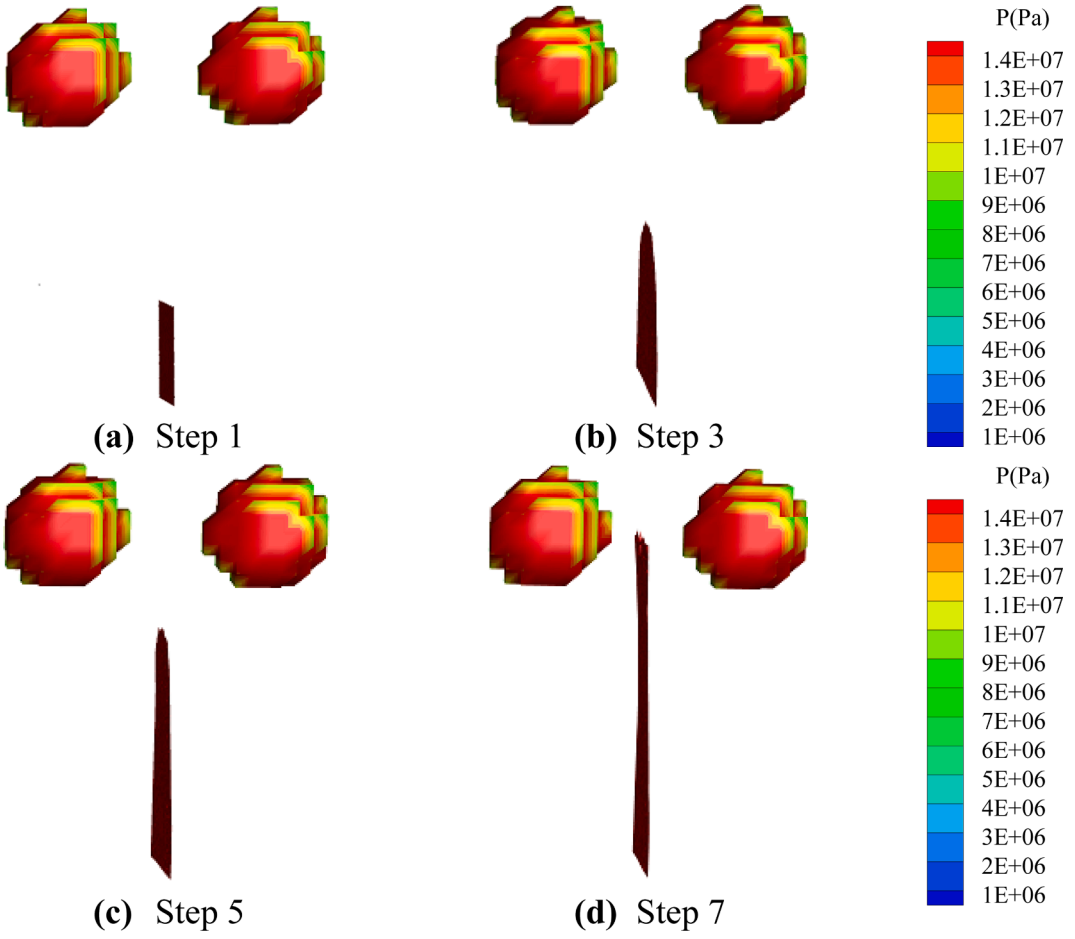



**Fig. 17.** The hydraulic fracture propagation path under the same cavity internal pressure in Model 5-II-a.

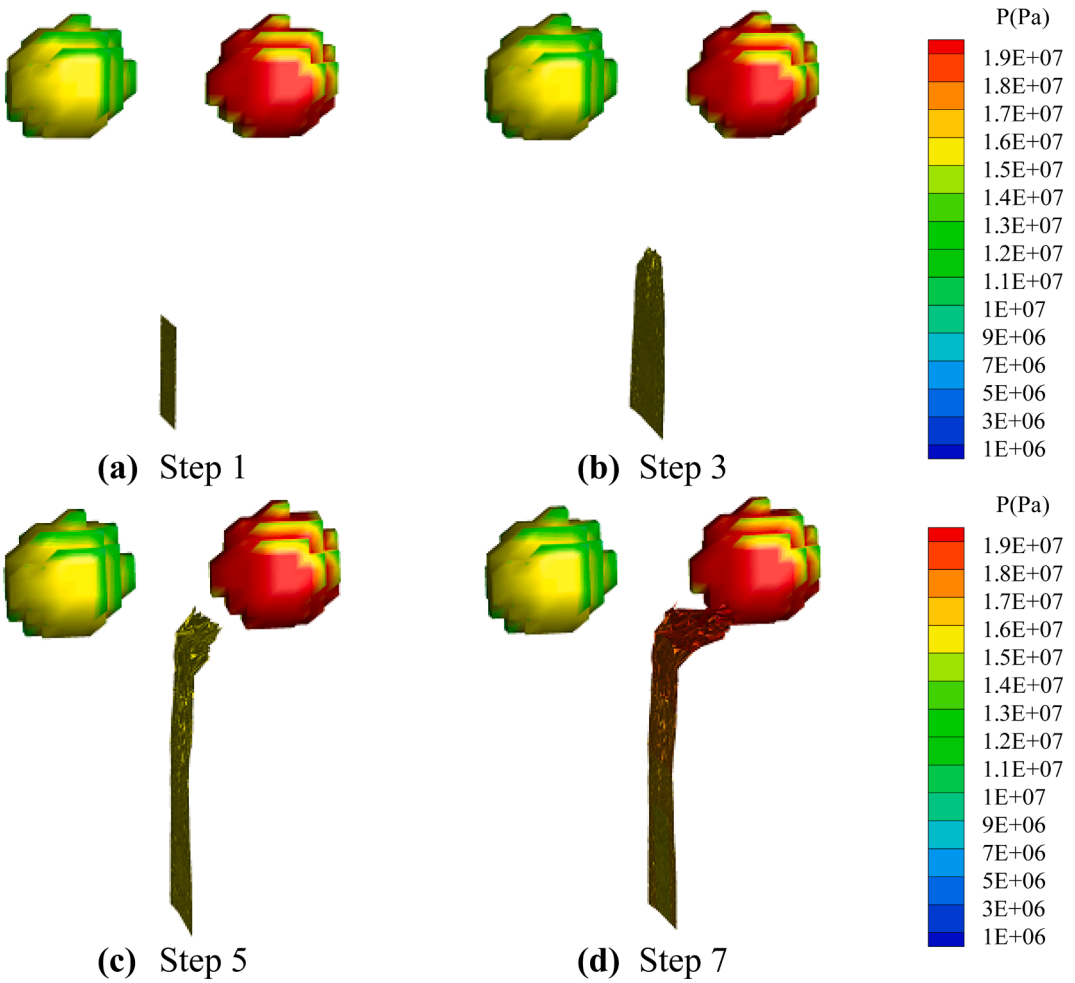



**Fig. 18.** The hydraulic fracture propagation path under different internal pressures of natural cavities in Model 5-II-b.

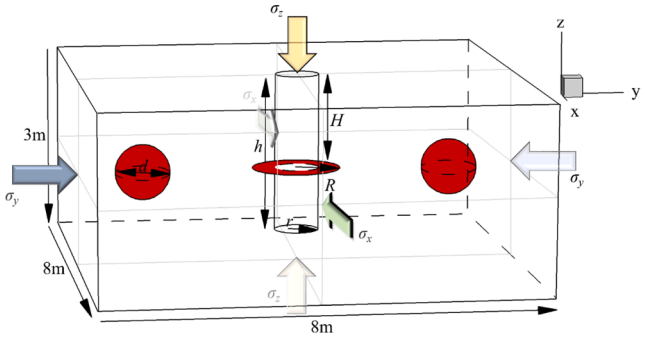



**Fig. 19.** The computational model of Model 6.

## 7. The coupling effect of multiple influencing factors

In this section, the coupling effects of natural fractures, natural cavities, confining stress and injection pressure at the wellbore are discussed. As shown in Fig. 22, in Model 7, the computational model is cubic with the dimension of 50 m × 50 m × 50 m. There are two oil-filled cavities. The distribution and strike angles of natural fractures are random, meanwhile the length of these natural fractures varies from 3 m to 5 m. The coordinates of these two cavities are (8, 25, 8) and (8, 25, 42) respectively, meanwhile the radius of two cavities is $r = 3$ m. A circular hydraulic fracture is located in the center of the computational model with a radius of $R = 4$ m. The confining stress is set to be $\sigma_x = 7$ MPa, $\sigma_y = 8$ MPa and $\sigma_z = 10$ MPa. The injection pressure of $p = 20$ MPa is applied on the surface of initial hydraulic fracture.

The cross-sectional view at $y = 20$ m of hydraulic fracture propagation in Model 7 is shown in Fig. 23. As shown in Fig. 23 (a) and (b), the hydraulic fracture initiates and propagates to the direction of maximum principal stress. As shown in Fig. 23 (c-e), when the hydraulic fracture connects with the natural fractures, the fluid flows into the natural fractures. Then, the natural fractures start to propagate. At this stage, the propagation of the hydraulic fracture is dominated by the natural fractures. As shown in Fig. 23 (f), the natural fractures propagate and turn to the direction of maximum principal confining stress, which finally connect to the natural cavity. During this process, the influence of natural fractures is the dominant. Without natural fractures, hydraulic fracture propagates and turns to the direction of maximum principal confining stress.

## 8. Conclusion

In carbonate fracture-cavity reservoirs, including Tahe oilfield, natural cavities are the main storage space of hydrocarbon. In order to enhance the connection between wellbores and hydrocarbon-filled cavities, it is critical to understand the propagation of hydraulic fractures in such a complex geological formation. In this work, the influence of natural fracture strike angle, natural cavity internal pressure, confining stress and injection pressure is studied using the TOUGH-AiFrac simulator. The following conclusions can be drawn:

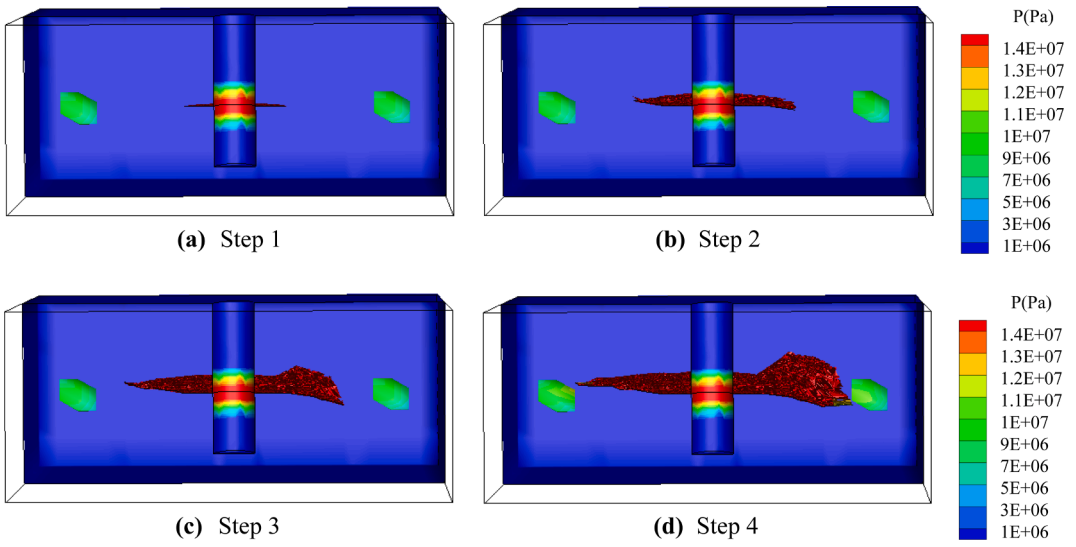



**Fig. 20.** The propagation path under injection pressure $p = 15$ MPa in Model 6-a.

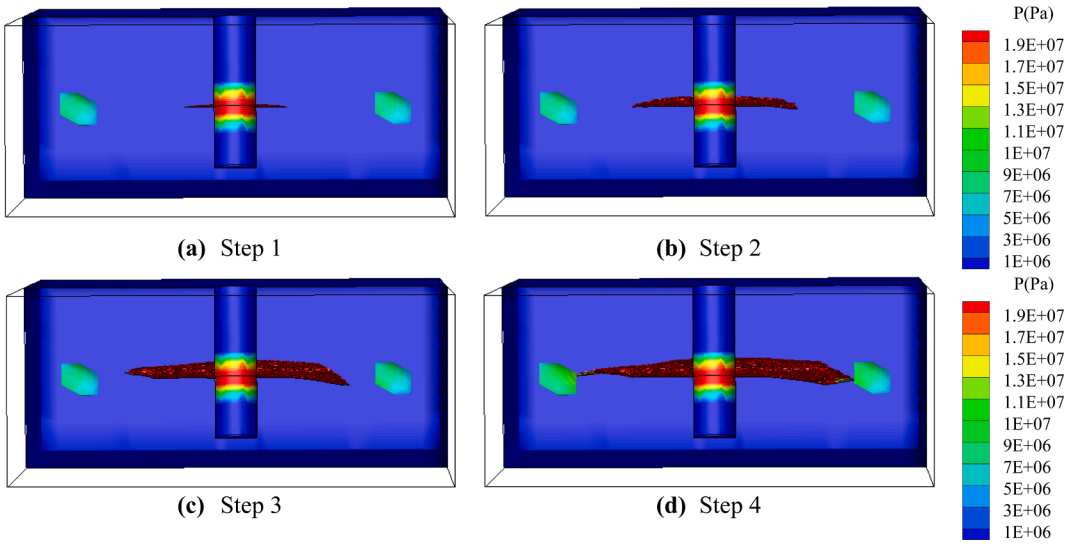



**Fig. 21.** The propagation path under injection pressure $p = 20$ MPa in Model 6-b.

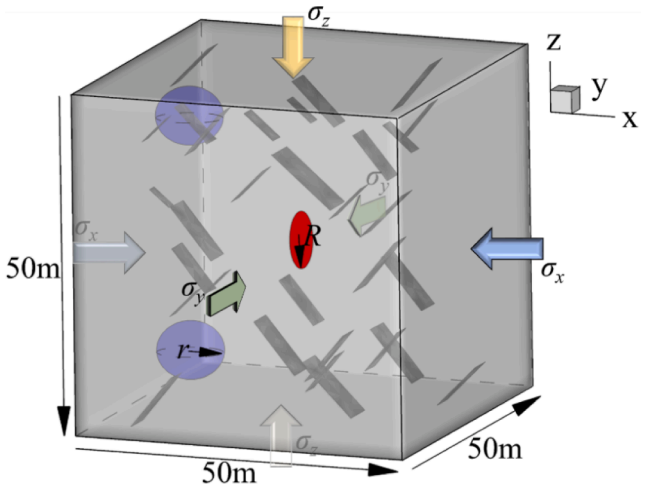



**Fig. 22.** The geometry of Model 7.

(1) Natural fractures have a significant influence on the path of hydraulic fracture propagation. According to the numerical results (see Model 3-II, Model 3-III and Model 3-IV), the orientation and distribution of natural fractures determine which natural cavity will connect with the production well.
(2) With confining stress, the hydraulic fracture propagates and turns to the direction of maximum principal stress. Without confining stress (see Model 4-I), the fracture propagates along the direction of initial hydraulic fracture and finally splits the sample into two parts. With confining stress (see Model 4-II), the hydraulic fracture propagates and turns to the direction of maximum principal stress and finally splits the sample into two parts.
(3) When the internal pressure of the natural cavities increases, the interaction between the hydraulic fracture and the cavities increases. The hydraulic fracture propagates and turns to the natural cavities with higher internal fluid pressure. The natural cavities with high internal fluid pressure have a strong attraction to the hydraulic fracture.
(4) When the injection fluid pressure increases, the hydraulic fracture becomes smoother, the influence of confining stress seems to decrease.

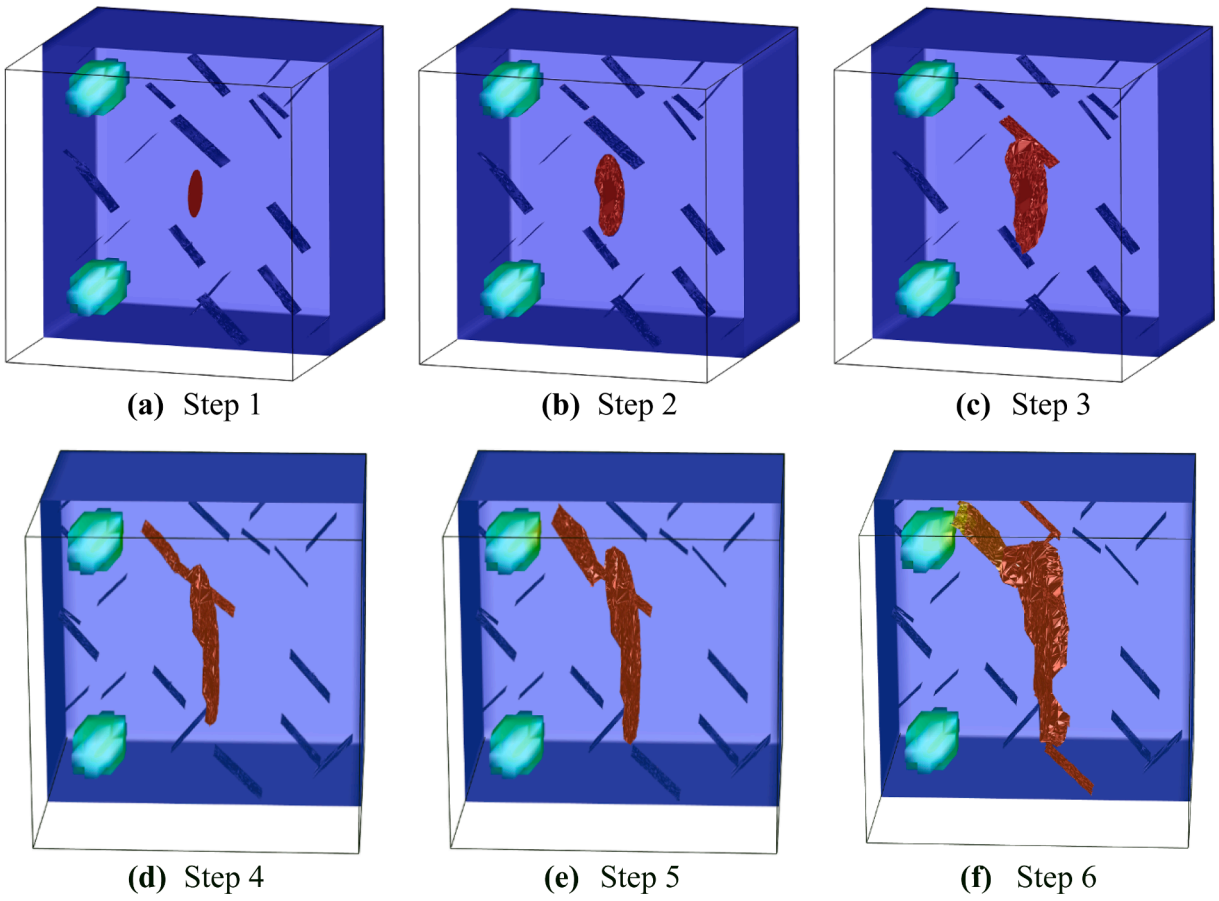



**Fig. 23.** The propagation of 3D hydraulic fracture with natural fractures and natural cavities under confining stress in Model 7.

(5) When multiple influencing factors are taken into account, the influence of natural fractures is dominant, which is followed by confining stress. These two influencing factors are critical for a successful hydraulic fracturing design. The fluid pressure in natural cavities and injection fluid pressure also have influence on the propagation of hydraulic fractures. However, in practical engineering, the injection fluid pressure that can be achieved is limited by the capacity of the equipment. Meanwhile, in Tahe oilfield, the internal pressure of the natural cavities is similar to the surrounding rock matrix (cavity pressure 0.9–1.1 times matrix pressure), so that they will not influence the propagation direction significantly.

## CRediT authorship contribution statement

**Jiangmei Qiao:** Writing – original draft. **Xuhai Tang:** Supervision, Methodology, Software, Writing – review & editing. **Mengsu Hu:** Investigation, Writing – review & editing. **Jonny Rutqvist:** Software, Writing – review & editing. **Zhiyuan Liu:** Conceptualization.

## Declaration of Competing Interest

The authors declare that they have no known competing financial interests or personal relationships that could have appeared to influence the work reported in this paper.

## Acknowledgement

The authors thank the support of the National Natural Science Foundation of China No.12172264.

## References

Ali, M.T., Ezzat, A.A., Nasr-EI-Din, H.H., 2019. A model to simulate matrix-acid stimulation for wells in dolomite reservoirs with vugs and natural fractures. SPE J. 25 (02), 609–631. https://doi.org/10.2118/199341-PA.

Beugelsdijk, L.J.L., Pater, C.J.D., Sato, K., 2000. Experimental hydraulic fracture propagation in a multi-fractured medium. In: SPE Asia Pacific Conference on Integrated Modelling for Asset Management, Yokohama, Japan, April. 10.2118/59419-MS.

Blanton, T.L., 1982. An experimental study of interaction between hydraulically induced and pre-existing fractures. In: SPE Unconventional Gas Recovery Symposium. https://doi.org/10.2118/10847-MS.

Cao, W.Z., Shi, J.Q., Durucan, S., Si, G.Y., Korre, A., 2020. Gas-driven rapid fracture propagation under unloading conditions in coal and gas outbursts. Int. J. Rock Mech. Min. Sci. 130, 104325. https://doi.org/10.1016/j.ijrmms.2020.104325.

Castonguay, S.T., Mear, M.E., Dean, R.H., Schmidt, J.H., 2013. Prediction of the growth of multiple interacting hydraulic fractures in three dimensions. In: SPE Annual Technical Conference and Exhibition, New Orleans, Louisiana, USA, 30 September-2 October. 10.2118/166259-MS.

Chalikakis, K., Plagnes, V., Guerin, R., Valois, R., Bosch, F.P., 2011. Contribution of geophysical methods to karst-system exploration: an overview. Hydrogeol. J. 19(6), 1169–1180. 10.1007/s10040-011-0746-x.

Chuprakov, D., Melchaeva, O., Prioul, R., 2014. Injection-sensitive mechanics of hydraulic fracture interaction with discontinuities. Rock Mech. Rock Eng. 47 (5), 1625–1640. https://doi.org/10.1007/s00603-014-0596-7.

Cipolla, C.L., Lolon, E.P., Erdle, J.C., Rubin, B., 2010. Reservoir modeling in shale-gas reservoirs. SPE Reservoir Eval. Eng. 13 (4), 638–653. https://doi.org/10.2118/125530-MS.

Guo, J.C., Zhao, X., Zhu, H.Y., Zhang, X.D., Pan, R., 2015. Numerical simulation of interaction of hydraulic fracture and natural fracture based on the cohesive zone finite element method. J. Nat. Gas Sci. Eng. 25, 180–188. https://doi.org/10.1016/j.jngse.2015.05.008.

Ishida, T., Aoyagi, K., Niwa, T., Chen, Y., Murata, S., Chen, Q.u., Nakayama, Y., 2012. Acoustic emission monitoring of hydraulic fracturing laboratory experiment with supercritical and liquid $CO_2$. Geophys. Res. Lett. 39 (16), n/a–n/a.

Izgec, O., Zhu, D., Hill, A.D., 2010. Numerical and experimental investigation of acid wormholing during acidization of vuggy carbonate rocks. J. Petrol. Sci. Eng. 74, 51–66. https://doi.org/10.1016/j.petrol.2010.08.006.

Jiang, H., Chen, M., Zheng, G.Q., Jin, Y., Zhao, Z.F., Zhu, G.F., 2009. Impact of oriented perforation on hydraulic fracture initiation and propagation. Chinese J. Rock Mech. Eng. 28 (7), 1321–1326 in Chinese.

Jiao, Y.Y., Zhang, H.Q., Zhang, X.L., Li, H.B., Jiang, Q.H., 2015. A two dimensional coupled hydromechanical discontinuum model for simulating rock hydraulic fracturing. Int. J. Numer. Anal. Meth. Geomech. 39, 457–481. https://doi.org/10.1002/nag.2314.

Kresse, O., Weng, X., Chuprakov, D., Prioul, R., Cohe, C., 2013. Effect of Flow Rate and Viscosity on Complex Fracture Development in UFM Model. In: Jeffrey, R. (Ed.), Effective and Sustainable Hydraulic Fracturing. InTech.

Li, Y., Hou, J.G., Li, Y.Q., 2016a. Features and classified hierarchical modeling of carbonate fracture-cavity reservoirs. Pet. Explor. Dev. 43 (4), 655–662. https://doi.org/10.1016/S1876-3804(16)30076-3.

Li, Y.Q., Hou, J.G., Ma, X.Q., 2016b. Data integration in characterizing a fracture-cavity reservoir, Tahe oilfield, Tarim basin. China. Arabian Journal of Geosciences. 9 (8), 1–12. https://doi.org/10.1007/s12517-016-2562-z.

Liu, Q.S., Sun, L., Tang, X.H., Chen, L., 2018a. Simulate intersecting 3D hydraulic cracks using a hybrid "FE-Meshfree" method. Eng. Anal. Boundary Elem. 91, 24–43. https://doi.org/10.1016/j.enganabound.2018.03.00 5.

Liu, Q.S., Sun, L., Tang, X.H., Guo, B., 2018b. Modelling hydraulic fracturing with a point-based approximation for the maximum principal stress criterion. Rock Mech. Rock Eng. 52 (6), 1781–1801. https://doi.org/10.1007/s006 03-018-1648-1.

Liu, Z.Y., Chen, M., Zhang, G.Q., 2014. Analysis of the influence of a natural fracture network on hydraulic fracture propagation in carbonate formations. Rock Mech. Rock Eng. 47 (2), 575–587. https://doi.org/10.1007/s00603 -013-0414-7.

Liu, Z.Y., Tang, X.H., Tao, S., Zhang, G.Q., Chen, M., 2020. Mechanism of connecting natural cavities and wells through hydraulic fracturing in fracture-cavity reservoirs. Rock Mech. Rock Eng. 53, 5511–5530. https://doi.org/10.1007/s00603-020-02225-w.

Liu, Z.Y., Wang, S.J., Zhao, H.Y., Wang, L., Li, W., Geng, Y.D., Tao, S., Zhang, G.Q., Chen, M., 2018c. Effect of random natural fractures on hydraulic fracture propagation geometry in fractured carbonate rocks. Rock Mech. Rock Eng. 51, 491–511. https://doi.org/10.1007/s00603-017-1331-y.

Lu, C., Luo, Y., Li, J.F., Chen, C., Xiao, Y.J., Liu, W., Lu, H.G., Guo, J.C., 2020. Numerical analysis of complex fracture propagation under temporary plugging conditions in a naturally fractured reservoir. SPE Prod. Oper. 35 (04), 0775–0796. https://doi.org/10.2118/201105-PA.

Lu, X.B., Wang, Y., Tian, F., Li, X.H., Yang, D.B., Li, T., Lv, Y.P., He, X.M., 2017. New insights into the carbonate karstic fault system and reservoir formation in the Southern Tahe area of the Tarim Basin. Mar. Pet. Geol. 86, 587–605. https://doi.org/10.1016/j.marpetgeo.2017.06.023.

Lucia, F.J., Kerans, C., Jr, J.W.J., 1999. Carbonate reservoir characterization. New York: Springer. 55(06), 70–72. 10.2118/82071-JPT.

Luo, Z.F., Zhang, N.L., Zhao, L.Q., Li, N., Ren, D.F., Liu, F., 2020. An extended finite element method for the prediction of acid-etched fracture propagation behavior in fractured-vuggy carbonate reservoirs. J. Petrol. Sci. Eng. 191, 107170 https://doi.org/10.1016/j.petrol.2020.107170.

Ma, G.W., Chen, Y., Jin, Y., Wang, H.D., 2018. Modelling temperature-influenced acidizing process in fractured carbonate rocks. Int. J. Rock Mech. Min. Sci. 105, 73–84. https://doi.org/10.1016/j.ijrmms.20 18.03.019.

Mendez, J.N., Jin, Q., Gonzalez, M., Zhang, X.D., Lobo, C., Boateng, C.D., Zambrano, M., 2020. Fracture characterization and modeling of karsted carbonate reservoirs: a case study in Tahe oilfield, Tarim Basin (western China). Mar. Pet. Geol. 112 (4), 104104 https://doi.org/10.1016/j.marpetgeo.2019.104104.

Olson, J.E., Taleghani, A.D., 2009. Modeling simultaneous growth of multiple hydraulic fractures and their interaction with natural fractures. In: SPE Hydraulic Fracturing Technology Conference, The Woodlands. https://doi.org/10.2118/119739-MS.

Pater, C.J.D., Beugelsdijk, L.J.L., 2005. Experiments and numerical simulation of hydraulic fracturing in naturally fractured rock. The 40th US Rock Mechanics Symposium on Rock Mechanics.

Peirce, A.P.P., Bunger, A.P.P., 2015. Interference Fracturing: nonuniform distributions of perforation clusters that promote simultaneous growth of multiple hydraulic fractures. SPE J. 20 (02), 384–395. https://doi.org/10.2118/172500-PA.

Potluri, N.K., Zhu, D., Hill, A.D., 2005. The effect of natural fractures on hydraulic fracture propagation. In: SPE European Formation Damage Conference, Sheveningen, the Netherlands, May 25. 10.2118/94568-MS.

Pruess, K., Oldenburg, C.M., Moridis, G.J., 2012. TOUGH2 User's Guide, Version 2.1. Rep. LBNL43134rev, Lawrence Berkeley National Laboratory, Berkeley, CA. 10.2172/751729.

Rahm, D., 2011. Regulating hydraulic fracturing in shale gas plays: The case of Texas. Energy Policy. 39 (5), 2974–2981. https://doi.org/10.1016/j.enpol.2011.03.009.

Rapoport, M.B., Rapoport, L.I., Ryjkov, V.I., 2004. Direct detection of oil and gas fields based on seismic inelasticity effect. Leading Edge. 23 (3), 276–278. https://doi.org/10.1190/1.1690901.

Rayudu, N.M., Tang, X., Singh, G., 2019. Simulating three dimensional hydraulic fracture propagation using displacement correlation method. Tunn. Undergr. Space Technol. 85, 84–91.

Rutqvis, J., 2017. An overview of TOUGH-based geomechanics models. Comput. Geosci. 108, 56–63. https://doi.org/10.1016/j.cageo.2016.09.007.

Rutqvist, J., Figueiredo, B., Hu, M.S., Tsang, C.-F., 2018. Continuum modeling of hydraulic fracturing in complex fractured rock masses. Hydraulic fracture modelling. 195–215 https://doi.org/10.1016/B978-0-12-812998-2.00007-2.

Rutqvist, J., Wu, Y.-S., Tsang, C.-F., Bodvarsson, G., 2002. A Modeling approach for analysis of coupled multiphase fluid flow, heat transfer, and deformation in fractured porous rock. Int. J. Rock Mech. Min. Sci. 39, 429–442. https://doi.org/10.1016/S1365-1609(02)00022-9.

Salimzadeh, S., Usui, T., Paluszny, A., Zimmerman, R.W., 2017. Finite element simulations of interactions between multiple hydraulic fractures in a poroelastic rock. Int. J. Rock Mech. Min. Sci. 99, 9–20. https://doi.org/10.1016/j.ijrmms.2017.09.001.

Tang, X.H., Rutqvist, J., Hu, M.S., Rayudu, N.M., 2019. Modeling three-dimensional fluid-driven propagation of multiple fractures using TOUGH-FEMM. Rock Mech. Rock Eng. 52, 611–627. https://doi.org/10.1007/s00603-018-1715-7.

Tao, S., Tang, X., Rutqvist, J., Liu, Q., Hu, M., 2021. The influence of stress anisotropy and stress shadow on frost cracking in rock. Comput. Geotech. 133, 103967. https://doi.org/10.1016/j.compgeo.2020.103967.

Tao, S.J., Tang, X.H., Rutqvist, J., Hu, M.S., Liu, Q.S., 2020. Simulating three dimensional thermal cracking with TOUGH-FEMM. Comput. Geotech. 124, 103654 https://doi.org/10.1016/j.compgeo.2020.103654.

Wang, X.G., Jardani, A., Jourde, H., 2017. A hybrid inverse method for hydraulic tomography in fractured and karstic media. J. Hydrol. 551, 29–46. https://doi.org/10.1016/j.jhydrol.2017.05.051.

Wang, Y.T., Zhou, X.P., Xu, X., 2016. Numerical simulation of propagation and coalescence of flaws in rock materials under compressive loads using the extended non-ordinary state-based peridynamics. Eng. Fract. Mech. 163, 248–273. https://doi.org/10.1016/j.engfracmech.2016.06.013.

Weng, X.W., Kresse, O., Cohen, C., Wu, R.T., Gu, H.R., 2011. Modeling of hydraulic-fracture-network propagation in a naturally fractured formation. SPE Prod. Oper. 26 (4), 368–380. https://doi.org/10.2118/140253-MS.

Wu, Y.S., Liu, H.H., Bodvarsson, G.S., 2004. A triple-continuum approach for modeling flow and transport processes in fractured rock. J. Contam. Hydrol. 73 (1/4), 145–179. https://doi.org/10.1016/j.jconhyd.2004.01.002.

Wu, Y.S., Yuan, D., Kang, Z.J., Fakcharoenphol, P., 2011. A multiple-continuum model for simulating single-phase and multiphase flow in naturally fractured vuggy reservoirs. J. Petrol. Sci. Eng. 78 (1), 13–22. https://doi.org/10.1016/j.petrol.2011.05.004.

Xu, C., Di, B.R., Wei, J.X., 2016. A physical modeling study of seismic features of karst cave reservoirs in the Tarim Basin China. Geophysics. 81 (1), B31–B41. https://doi.org/10.1190/geo2014-0548.1.

Xu, J.J., Tang, X.H., Wang, Z.Z., Feng, Y.F., Bian, K., 2020. Investigating the softening of weak interlayers during landslides using nanoindentation experiments and simulations. Eng. Geol. 277, 105801 https://doi.org/10.1016/j.enggeo.2020.105801.

Yan, C.Z., Zheng, H., Sun, G.H., Ge, X.R., 2016. Combined finite-discrete element method for simulation of hydraulic fracturing. Rock Mech. Rock Eng. 49 (4), 1389–1410. https://doi.org/10.1007/s00603-015-0816-9.

Yang, Y.T., Tang, X.H., Zheng, H., Liu, Q.S., Liu, Z.J., 2018. Hydraulic fracturing modelling using the enriched numerical manifold method. Appl. Math. Model. 53, 462–486. https://doi.org/10.1016/j.apm.2017.09.024.

Yang, Y.T., Xu, D.D., Liu, F., Zheng, H., 2020. Modeling the entire progressive failure process of rock slopes using a strength-based criterion. Comput. Geotech. 126, 103726 https://doi.org/10.1016/j.compgeo.2020.103726.

Zhang, F.S., Damjanac, B., Maxwell, S., 2019. Investigating hydraulic fracturing complexity in naturally fractured rock masses using fully coupled multiscale numerical modeling. Rock Mech. Rock Eng. 52 (12), 5137–5160. https://doi.org/10.1007/s00603-019-01851-3.

Zhang, F.S., Dontsov, E., Mack, M., 2017. Fully coupled simulation of hydraulic fracture interacting with natural fractures with a hybrid discrete-continuum method. Int. J. Numer. Anal. Methods Geomech. 41 (13), 1430–1452. https://doi.org/10.1002/nag.2682.

Zhang, M.Z., Liu, Z.Y., Jiang, Q., He, B.G., 2021. Influence of natural cavities on hydraulic fracturing pressure curves: numerical modelling and ANNs. Arabian J. Geosci. 14, 2135. https://doi.org/10.1007/s12517-021-08437-w.

Zhao, Q., Lisjak, A., Mahabadi, O., Liu, Q.Y., Grasselli, G., 2014. Numerical simulation of hydraulic fracturing and associated microseismicity using finite-discrete element method. J. Rock Mech. Geotech. Eng. 6 (006), 574–581. https://doi.org/10.1016/j.jrmge.2014.10.003.

Zheng, H., Yang, Y.T., Shi, G.H., 2019. Reformulation of dynamic crack propagation using the numerical manifold method. Eng. Anal. Boundary Elem. 105, 279–295. https://doi.org/10.1016/j.enganabound.2019.04.023.

Zhou, J., Chen, M., Yan, J., Zhang, G.Q., 2008. Analysis of fracture propagation behavior and fracture geometry using a tri-axial fracturing system in naturally fractured reservoirs. Int. J. Rock Mech. Min. Sci. 45 (7), 1143–1152. https://doi.org/10.1016/j.ijrmms.2008.01.001.

Zhou, J., Jin, Y., Chen, M., 2010. Experimental investigation of hydraulic fracturing in random naturally fractured blocks. Int. J. Rock Mech. Min. Sci. 47 (7), 1193–1199. https://doi.org/10.1016/j.ijrmms.2010.07.005.

Zhou, L.B., Guo, A.B., Wang, X.G., Qiao, J.M., Tang, X.H., 2022. The effect of temperature, natural fractures and vugs on the acidizing process in fractured-vuggy reservoirs with hydro-thermal-chemical coupled modeling. J. Petrol. Sci. Eng. 213, 110416 https://doi.org/10.1016/j.petrol. 2022.110416.

Zhu, H.Y., Deng, J.G., Jin, X.C., Hu, L.B., Luo, B., 2015. Hydraulic fracture initiation and propagation from wellbore with oriented perforation. Rock Mech. Rock Eng. 48 (2), 585–601. https://doi.org/10.1007/s00603-014-0608-7.

Zhuang, L., Kim, K.Y., Jung, S.G., Diaz, M., Min, K.B., 2019. Effect of water infiltration, injection rate and anisotropy on hydraulic fracturing behavior of granite. Rock Mech. Rock Eng. 52(2), 575–589. https://doi. org/10.1007/s00603-018-1431-3.